Macromolecules

Cite This: Macromolecules 2019, 52, 6734−6740

Article

pubs.acs.org/Macromolecules

End-on Chain Orientation of Poly(3-alkylthiophene)s on a Substrate by Microphase Separation of Lamellar Forming Amphiphilic Diblock Copolymer

Kyu Seong Lee,[†] Philgon Kim,[†] Jaeyong Lee,[†] Chungryong Choi,[†] Yeseong Seo,[†] So Yeong Park,[†] Keonwoo Kim,[†] Chaneui Park,[‡] Kilwon Cho,[‡] Hong Chul Moon,[§] and Jin Kon Kim*[,†]

[†]National Creative Research Initiative Center for Smart Block Copolymers, Department of Chemical Engineering, and [‡]Department of Chemical Engineering, Pohang University of Science and Technology, Pohang, Kyungbuk 37673, Republic of Korea

[§]Department of Chemical Engineering, University of Seoul, Seoul 02504, Republic of Korea

Supporting Information

ABSTRACT: We obtained the end-on orientation of poly(3-dodecylthiophene) (P3DDT) chains where the main chains are vertically oriented on a substrate by synthesizing poly(3-dodecylthiophene)-*block*-poly(3-(2-(2-(2-methoxyethoxy)-ethoxy)ethoxy)methyl thiophene) copolymer (P3DDT-*b*-P3TEGT) with two different weight fractions of P3DDT block (w_{P3DDT} = 0.48 and 0.65). Both block copolymers showed well-ordered lamellar microdomains in bulk, verified by small-angle X-ray scattering (SAXS). Because of the high incompatibility of the two blocks, P3DDT-*b*-P3TEGT thin films prepared by spin-coating on a substrate followed by thermally annealing showed parallel oriented lamellar microdomains to the substrate. Hydrophilic P3TEGT microdomains were located at the substrate/polymer interface, while hydrophobic P3DDT microdomains were located at the polymer/air interface. Thus, both P3DDT and P3TEGT backbone chains were oriented perpendicularly to the lamellar layer (namely, film thickness direction), and the end-on orientations of P3DDT and P3TEGT chains were obtained. The hole mobility was measured by fabricating a space-charge-limited current (SCLC) device. P3DDT-*b*-P3TEGT showed much enhanced mobility compared with the device made of neat P3DDT film with edge-on orientation, indicating that end-on orientation is very effective for improving the hole mobility along the vertical direction.

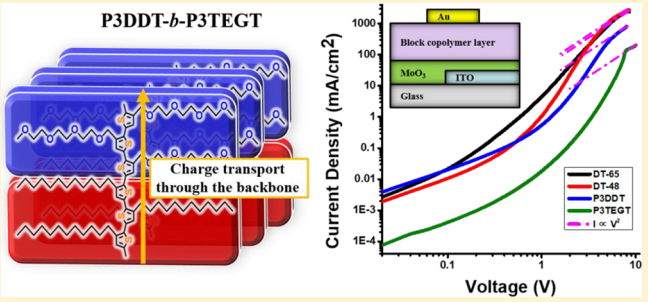

INTRODUCTION

Polymer-based organic electronic devices have received great attention due to their application to flexible and lightweight electronic devices.[1−8] Among many conducting polymers, poly(3-alkylthiophene)s (P3ATs) have been widely used as conducting polymers in organic field-effect transistors,[1−3] organic photovoltaics,[4,5] and chemical sensors[6] because of high charge carrier mobility and good solubility in organic solvents in addition to easy synthesis.

To improve the performance of conducting polymer-based organic electronic devices, the control of the nanostructure of the conducting polymers and the polymer chain arrangement are very important[9−12] because those affect significantly the pathway of holes (or electrons).[12,13]

Scheme 1 shows three chain orientations (edge-on, face-on, and end-on) in P3AT thin films. Pathways of holes in each orientation of P3AT chains are (1) alkyl side chain direction [(100) plane], (2) $\pi-\pi$ stacking direction [(010) plane], and (3) the main-chain direction [(001) plane]. Among the three orientations, hole mobility along the vertical direction of a film, which is the critical factor for a vertically operating device,[12−14] is the highest when the main chains are aligned vertically (end-on orientation), while it is the lowest when the side chains are aligned vertically (edge-on orientation).[12,13] However, most P3ATs in films reported in the literature showed edge-on orientation due to the low surface energy of the alkyl side chain,[15−19] although face-on orientation could be obtained through modification of the substrate surface.[19,20]

Some research groups have attempted to obtain end-on orientation of conducting polymers.[12,14] Tajima et al. fabricated end-functionalized poly(3-butylthiophene) (P3BT) with a fluoroalkyl group (P3BT-F).[12] Because of the self-segregation of fluoroalkyl groups, P3BT-F showed end-on orientation on the top surface. However, edge-on orientation was also present at the substrate/polymer interface. Hu et al. fabricated end-on orientation of poly(3-hexylthiophene) (P3HT) using nanoimprinting lithography.[14] However, end-on orientation of P3HT was only present in the nanoimprinted structure, whereas nonimprinted area in the film still showed edge-on orientation.

Received: June 19, 2019
Revised: August 20, 2019
Published: August 28, 2019

DOI: 10.1021/acs.macromol.9b01266
Macromolecules 2019, 52, 6734−6740

Scheme 1. Schematic of (a) Edge-on, (b) Face-on, and (c) End-on Orientations in P3AT Thin Films

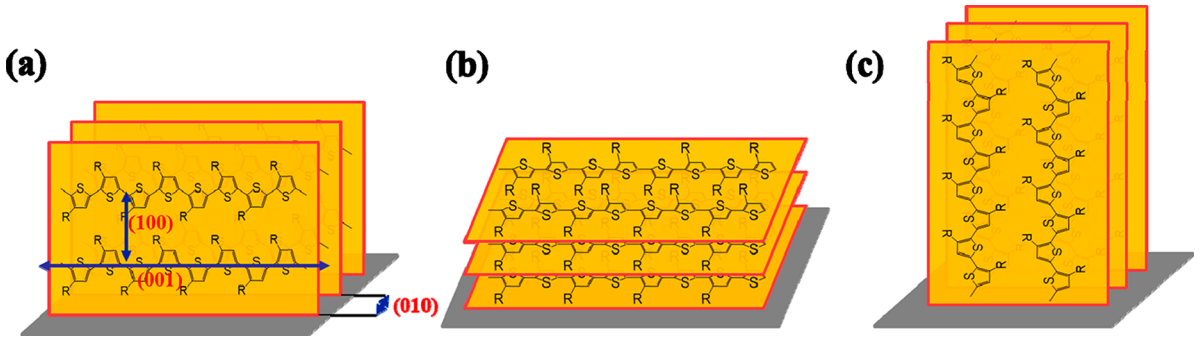

In this study, we utilized the self-assembly of block copolymers to fabricate end-on orientation of P3ATs. When the thickness (t) of a thin film of a block copolymer with lamellar microdomains is commensurable with the lamellar domain spacing (L_0), the lamellar microdomains are parallel oriented to a substrate. For parallel oriented microdomains, P3AT backbone chains in P3AT-contaning block copolymers should be aligned along the lamellar layer (i.e., the film thickness direction), as shown in Scheme 2. Because most block copolymers consisting of P3HT showed only fibril structure due to a strong rod−rod interaction of P3HT,[21−25] the rod−rod interaction of the P3AT should be reduced to obtain well-ordered lamellar microdomains, We previously reported that the polystyrene-*b*-poly(3-dodecylthiophene) copolymer (PS-*b*-P3DDT) showed parallel oriented lamellar microdomains.[26] However, we could not use PS-*b*-P3DDT for organic electronic devices because PS is not a conducting polymer. In this study, we used amphiphilic diblock copolymers consisting of hydrophobic P3DDT and hydrophilic poly(3-(2-(2-(2-methoxyethoxy)ethoxy)ethoxy)-methylthiophene) (P3TEGT) blocks to increase the incompatibility between two blocks to form well-ordered lamellar microdomains. P3DDT-*b*-P3TEGTs with two different weight fractions of P3DDT block (w_{P3DDT} = 0.48 and 0.65) showed lamellar microdomains in bulk. All thin films showed parallel oriented lamellar microdomains to the substrate. This is because of a large difference of surface tension between hydrophobic P3DDT and hydrophilic P3TEGT. We found via grazing incidence wide-angle X-ray scattering (GIWAXS) that P3DDT and P3TEGT chains had end-on orientation. Because of this orientation, the hole mobility of P3DDT-*b*-P3TEGTs along the film thickness direction was greatly enhanced (more than 10 times) compared with P3DDT neat film with edge-on orientation.

Scheme 2. Schematic of End-on Orientation of P3DDT-*b*-P3TEGT Chains with Parallel Orientated Lamellar Microdomains on a Substrate[a]

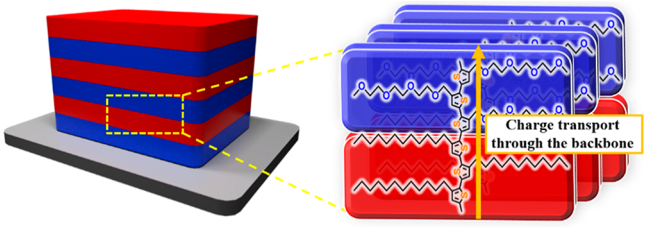

[a]Blue and red areas represent P3TEGT and P3DDT microdomains.

Scheme 3. Synthetic Routes of (a) TEGT Monomer (3), (b) P3TEGT (4), (c) P3DDT (5), and (d) P3DDT-*b*-P3TEGT (6)

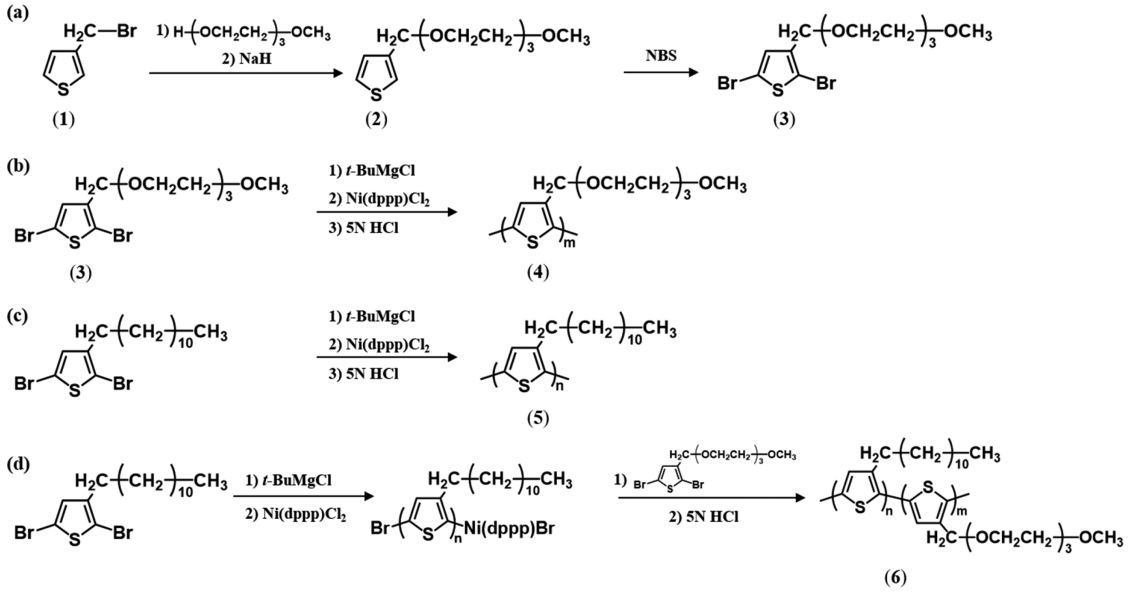

DOI: 10.1021/acs.macromol.9b01266
Macromolecules 2019, 52, 6734−6740

Table 1. Molecular Characteristics of Homopolymers and Block Copolymers Employed in This Study

sample[a]	$M_{n,total}$[b]	$Đ$[b]	w_{P3DDT}[c] ($M_{n,P3DDT}$)[b]	w_{P3TEGT}[c] ($M_{n,P3TEGT}$)[b]	T_m[d](P3DDT) (°C)	T_m[d](P3TEGT) (°C)
P3TEGT	26000	1.25		1.00		97
DT-48	19500	1.35	0.48 (9400)	0.52 (10100)	146	ND[e]
DT-65	23000	1.35	0.65 (15000)	0.35 (8000)	154	ND[e]
P3DDT	12500	1.13	1.00		149	

[a]X in DT-X indicates the weight percentage of P3DDT block. [b]Determined by SEC based on PS standards. [c]Measured by ^{1}H NMR. [d]Measured from the peak of DSC thermograms. [e]Not detected.

EXPERIMENTAL SECTION

Materials. 2,5-Dibromo-3-dodecylthiophene was purchased from Tokyo Chemical Industry Co. and purified by silica column with *n*-hexane. 3-Bromothiophene was purchased from AstaTech, Inc. Other chemicals including triethylene glycol monomethyl ether, sodium hydride (NaH, 60% dispersion in mineral oil), and *N*-bromosuccinimide (NBS) were used as received from Aldrich Chemical Co. Synthetic details of P3TEGT monomer, P3TEGT homopolymer, P3DDT homopolymer, and P3DDT-*b*-P3TEGTs are described in the Supporting Information (Scheme 3).[21,27]

Characterization. The number-average molecular weight (M_n) and polydispersity index ($Đ$) of all polymers were measured by size exclusion chromatography (SEC: Waters 2414 refractive index detector) with two 300 mm (length) × 7.5 mm (inner diameter) columns, including particle size of 5 μm (PL gel 5 μm MIXED-C: Polymer Laboratories) with THF as an eluent and a flow rate of 1 mL/min at 35 °C. End-functionalization of all polymers was checked by ^{1}H nuclear magnetic resonance spectra (^{1}H NMR: Bruker digital AVANCE III 400 MHz) with chloroform-*d* ($CDCl_3$) as a solvent. The weight fraction of P3DDT (w_{P3DDT}) was determined by ^{1}H NMR based on the characteristic peaks of P3DDT (δ = 2.5−2.8 ppm) and P3TEGT (δ = 4.4−4.8 ppm) (Figure S1). All synthesized P3DDT-*b*-P3TEGTs as well as P3DDT and P3TEGT homopolymers showed narrow molecular weight distribution (Figure S2). The molecular characteristics of all the samples are summarized in Table 1.

Small-Angle and Wide-Angle X-ray Scattering (SAXS and WAXS). SAXS and WAXS profiles ($I(q)$ vs q (= $(4\pi/\lambda)$ sin θ), where q and 2θ are the scattering vector and scattering angle, respectively) were obtained on beamline 4C at the Pohang Accelerator Laboratory (South Korea). The wavelength and beam size were 0.675 Å and 0.2 (H) × 0.6 (W) mm^2, respectively. A two-dimensional charge-coupled detector (Mar USA, Inc.) was employed. The sample-to-detector distance was 4 m for SAXS and 0.2 m for WAXS. The thickness of samples for SAXS and WAXS was 1 mm.

Differential Scanning Calorimetry (DSC). The thermal properties of all polymers after thermal annealing were measured by using a PerkinElmer DSC 4000. Calibration was conducted with zinc and indium. The sample (~5 mg) was first heated to 200 °C and annealed at 200 °C for 10 min to remove thermal history. Then, it was cooled to −30 °C and crystallized at this temperature for 10 min. Finally, DSC thermograms were obtained by the second heating from −30 to 200 °C. All heating and cooling cycles were performed at a rate of 10 °C/min.

Thin Film Preparation. Thin films were prepared by spin-coating of 0.5−2.0 wt % toluene solution by changing rotating speed (rpm) to adjust film thickness on a pristine silicon wafer. The thickness of all block copolymer thin films was measured by an ellipsometer (M-2000 V, J.A. Woollam Co.). Films were dried in a vacuum at room temperature and then annealed at various temperatures and followed by slow cooling to room temperature. The surface morphology of block copolymer thin films was investigated by tapping mode atomic force microscopy (AFM, Veeco DI dimension 3100 with Nanoscope V).

Grazing-Incidence Small-Angle (and Wide-Angle) X-ray Scattering (GISAXS and GIWAXS). GISAXS experiments were performed at room temperature on beamline 3C at the PAL to investigate the morphology of thin film through the entire thickness. The operating wavelength was 0.15 nm. The sample-to-detector distance was 4 m. The incident angle (α_i) was set at 0.16°. GIWAXS experiments were performed on the same line, but the sample-to-detector distance was 0.2 m.

X-ray Reflectivity (XRR). XRR experiments were performed at room temperature on beamline 5A at the PAL to investigate the morphology of thin film through the entire thickness. The operating wavelength was 0.15 nm.

Space-Charge-Limited Current (SCLC) Device Fabrication. The SCLC devices were fabricated as follows. First, MoO_3 with a thickness of 9 nm was deposited on an ITO-coated glass substrate followed by thermal treatment 120 °C for 1 h under vacuum. Then, a block copolymer solution in toluene was spin-coated and annealed at 190 °C for 1 h under vacuum, followed by slow cooling to room temperature. The thickness of block copolymer layers was ~100 nm measured by AFM. Finally, a gold electrode was deposited. J−V curves were obtained by using a Keithley 4200. From J−V curves, the hole mobility (μ) was extracted by fitting with Mott−Gurney equation:

$$J = \frac{9}{8}\varepsilon\varepsilon_0\mu\frac{V^2}{L^3}$$

in which ε_0 is the permittivity of free space (8.85×10^{-12} F m^{-1}), L is the thickness of the block copolymer layer, and ε is the dielectric constant of the block copolymer and assumed to be the same (3.0) for all samples.

RESULTS AND DISCUSSION

Figure 1 shows SAXS and WAXS profiles at various temperatures for DT-48 in bulk. The SAXS profile (Figure 1a) shows characteristic peaks at the position of 1:2:3 relative to the first-order peak (q^* = 0.283 nm^{-1}, the lamellar domain spacing (L_0) = $2\pi/q^*$ = 22.2 nm), indicating that DT-48 showed lamellar microdomains at all temperatures.

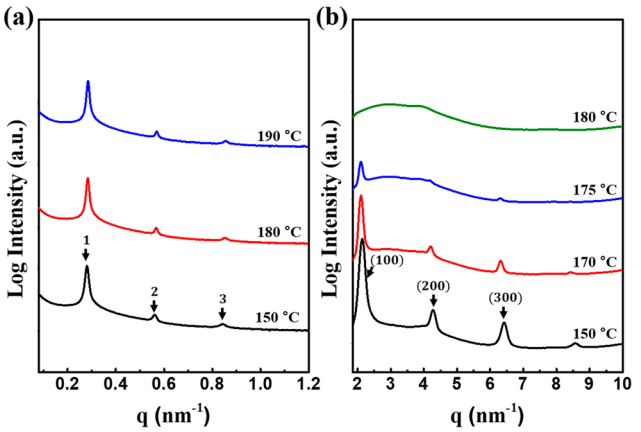

Figure 1. (a) SAXS and (b) WAXS profiles at various temperatures for DT-48 in bulk.

The WAXS profile (Figure 1b) at 150 °C clearly shows (100), (200), and (300) crystal peaks for P3DDT. The position of peaks exactly corresponded to those of neat

DOI: 10.1021/acs.macromol.9b01266
Macromolecules 2019, 52, 6734−6740

P3DDT homopolymer (Figure S3). At 180 °C, all the crystals corresponding to (100), (200), and (300) peaks of P3DDT disappeared. This temperature is ~20 °C higher than the final melting point of P3DDT block in DT-48 measured by DSC (see Figure S4). A similar behavior was observed for the poly(3-hexyl thiophene)-*b*-poly(2-vinylpyridine) copolymer.[28] SAXS and WAXS profiles of DT-65 at various temperatures are given in Figure S5, where DT-65 also shows the lamellar microdomains.

Figure 2 shows AFM height and phase images of DT-48 with two different film thicknesses before and after thermal annealing at 190 °C for 1 h. When DT-48 thin films were annealed at 190 °C, the hole−island structure was observed at a film thickness (t) of $2.0L_0$, whereas it was not found at t of $1.5L_0$. When a block copolymer thin film with lamellar microdomains has parallel orientation to the substrate, the hole−island structure is formed when t is incommensurable with L_0.[29,30] Because of the hydrophobic P3DDT and hydrophilic P3TEGT, the P3DDT block is located at the air surface and the P3TEGT block is located near the substrate side, namely, asymmetric wetting. In this situation, the commensurability is satisfied at $t = (n + 1/2)L_0$, where n is the integer. The formation of the hole−island structure at incommensurable film thickness ($t = 2.0L_0$) as shown in Figure 2c indicates that DT-48 thin films should have parallel oriented lamellar microdomains. Interestingly, P3DDT fibrils are clearly observed in phase contrast AFM images at both thicknesses. The formation of P3DDT fibrils at the film surface is attributed to the fact that the molecular weight of P3DDT block is large for the formation of folding of P3DDT chains.[26,31,32] When the hydrophobic P3DDT chains with a large molecular weight maintain the end-on orientation without chain folding up to the air/polymer surface, the coverage of P3DDT chains at the air surface would be small, which results in a large enthalpic penalty. Thus, fibril structures with edge-on orienation capable of covering a large area are preferred near the top of the film surface.

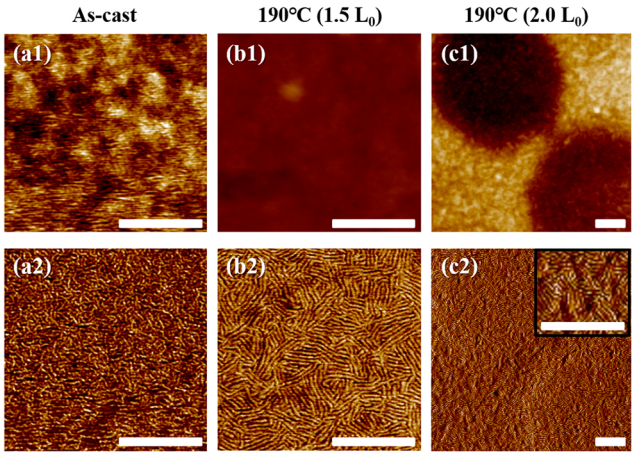

Figure 2. AFM height (upper panels) and phase contrast (lower panels) images of DT-48 at two different film thicknesses (a, b: t = 33.1 nm ($1.5L_0$), c: t = 44.6 nm ($2.0L_0$) before (a) and after thermal annealing at 190 °C for 1 h (b, c), followed by slow cooling to room temperature. The scale bar in all images is 400 nm.

X-ray reflectivity (XRR) experiments were performed to investigate the out-of-plane orientation of DT thin films (Figure S7). The XRR profiles showed characteristic Bragg peaks at the position of 1:2:3 relatives to the first-order peaks, indicating that DT thin films had lamellar structures with the lamellar plane parallel to the substrate.[33,34] The parallel oriented lamellar microdomains of DT-65 thin film were further confirmed by GISAXS experiment (Figure S8). The

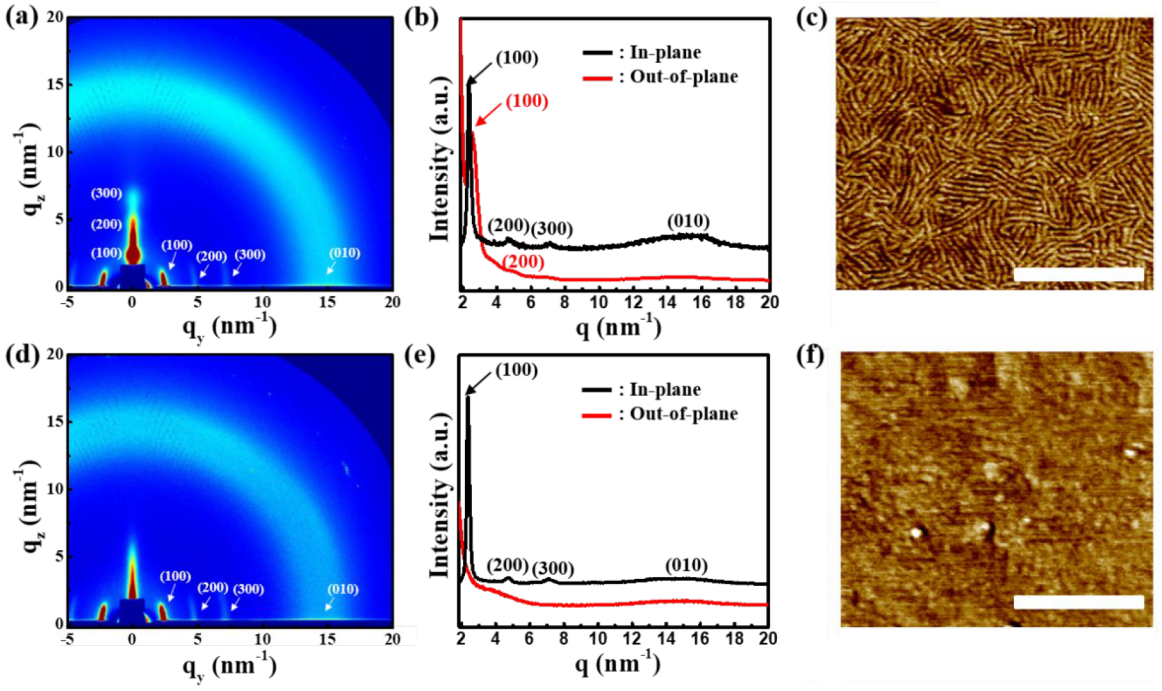

Figure 3. (a, d) GIWAXS patterns, (b, e) in-plane and out-of-plane scans of GIWAXS, and (c, f) AFM phase contrast image of thermally annealed DT-48 thin film (t = 33.1 nm ($1.5L_0$)). The sample was annealed at 190 °C, followed by slow cooling to room temperature. The upper and lower panels represent before and after reactive-ion etching. The scale bar in all images is 400 nm.

DOI: 10.1021/acs.macromol.9b01266
Macromolecules 2019, 52, 6734−6740

GISAXS profile showed diffuse Bragg sheets (DBSs) along the out-of-plane direction which came from lamellar microdomains oriented parallel to the substrate.[35] In addition, any peak was not observed along the in-plane direction. Thus, DT thin film had parallel oriented lamellar microdomains.

We performed GIWAXS experiments to investigate the orientation of crystalline structures of DT thin film. GIWAXS patterns for P3DDT and P3TEGT homopolymers were also obtained for the comparison (Figure S9). After thermal annealing, neat P3DDT and P3TEGT films showed edge-on orientation, consistent with previous reports.[36] The crystalline packing distances measured by GIWAXS were well matched with those measured by WAXS in bulk (q^* = 2.28 nm^{-1} for P3DDT and q^* = 2.65 nm^{-1} for P3TEGT).

Figure 3 shows GIWAXS results and AFM phase contrast images of thermally annealed DT-48 thin film before and after reactive-ion etching (RIE). Before RIE, the GIWAXS pattern of DT-48 showed (100), (200), and (300) crystal peaks of P3DDT chains along the in-plane direction. Those peaks indicated that P3DDT chains had well-ordered end-on orientation, where P3DDT backbone chains were oriented to the vertical direction of the film, and thus the crystals were packed along the (100) direction.[36] However, crystal peaks along the out-of-plane were also observed, suggesting that P3DDT chains in P3DDT fibrils had edge-on orientation. To confirm the chain orientation at the top film surface more clearly, the GIWAXS pattern was obtained after O_2 RIE for annealed film at 190 °C. O_2 RIE was performed at 100 sccm and 30 W for 5 s, which etched 4 nm of the film. In this situation, the edge-on orientation of P3DDT resulting from the P3DDT fibrils, which was seen in the out-of-plane for the sample without RIE, was completely removed. The absence of P3TEGT crystal peaks in GIWAXS for P3DDT-*b*-P3TEGT thin film was ascribed to much stronger crystal peaks of P3DDT than relatively weak crystal peaks of P3TEGT. To confirm the chain orientation of P3TEGT, we removed most P3DDT layers of DT-48 film by using O_2 RIE. In this situation, the final film thickness of DT-48 film was reduced to 10 nm (Figure S10a). We obtained GIWAXS pattern of this sample (Figure S10b). It was clearly seen in Figure S10 that the end-on orientation of P3TEGT was observed along the in-plane direction, which was not seen in the in-plane scan for the sample without RIE due to the strong crystal peaks of P3DDT. Also, because of the absence of crystal peaks belonging to both P3DDT and P3TEGT chains along the out-of-plane direction, both P3DDT and P3TEGT backbone chains in the DT film had end-on orientation. Namely, both chains were oriented perpendicularly to the interface of two blocks except a top film surface covered by P3DDT fibrils.[21,37] The GIWAXS pattern of DT-65 thin film without RIE exhibited almost the same as DT-48 (Figure S11). Based on the above results, the alignment of P3DDT and P3TEGT chains in DT-48 thin film is schematically shown in Figure 4.[26,38]

Finally, we measured hole mobility (μ) of two DTs by fabricating SCLC devices. The $J-V$ curves are shown in Figure 5. The average hole mobility (in $cm^2\ V^{-1}\ s^{-1}$) of each polymer calculated from the $J-V$ curves was as follows: $(1.71 \pm 0.03) \times 10^{-5}$ for DT-48, $(1.65 \pm 0.10) \times 10^{-5}$ for DT-65, $(1.52 \pm 0.15) \times 10^{-6}$ for neat P3DDT, and $(5.71 \pm 0.93) \times 10^{-7}$ for neat P3TEGT. Interestingly, μ of DT-48 and DT-65 was almost 1 order of magnitude higher than that of neat P3DDT with edge-on orientation, even though low μ of P3TEGT was existent in both DTs. This was mainly due to the end-on

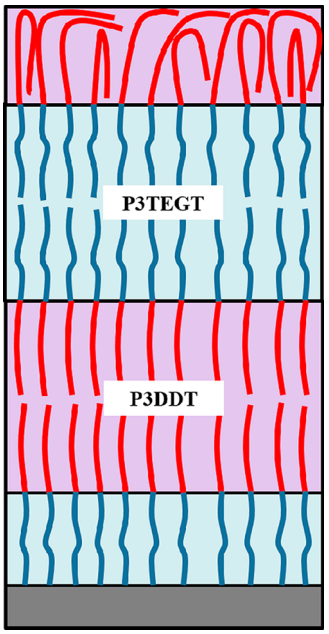

Figure 4. Schematic of chain alignments in P3DDT and P3TEGT chains in DT-48 at $t = 1.5L_0$.

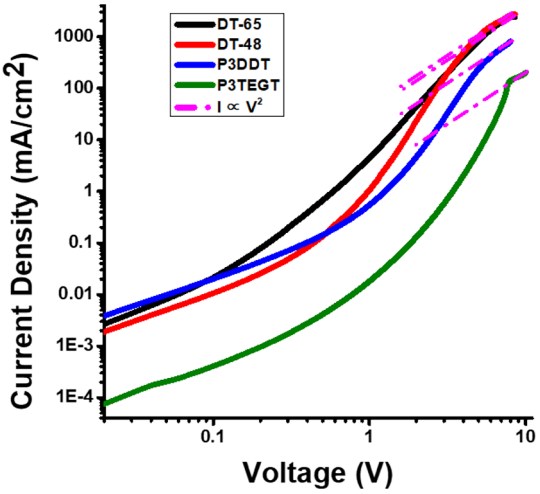

Figure 5. Current density versus voltage ($J-V$) curves of the space-charge-limited current (SCLC) device for the hole mobility measurement of P3DDT and P3TEGT homopolymers as well as DT-48 and DT-65.

orientation of P3DDT as well as P3TEGT in DT-48 and DT-65. Although μ corresponding to end-on orientation ($\mu_{end\text{-}on}$) is definitely higher than that corresponding to edge-on orientation ($\mu_{edge\text{-}on}$), it is not easy to calculate the exact value of $\mu_{end\text{-}on}$ from our experimental results because edge-on orientation still exists at the top of the DT film. However, when we employ the Matthiessen method,[39] the estimated $\mu_{end\text{-}on}$ of DT-48 and DT-65 is ~37 and ~30 times larger than $\mu_{edge\text{-}on}$ of DT-48 and DT-65, respectively (a detailed procedure is given in Figure S12 and Table S1), which is consistent with previous reports that the charge transport of end-on orientation through the conducting polymer backbone chains was 30 times faster than that of edge-on orientation.[12,13]

DOI: 10.1021/acs.macromol.9b01266
Macromolecules 2019, 52, 6734−6740

CONCLUSIONS

In this study, we synthesized P3DDT-*b*-P3TEGT (DT) with two different P3DDT weight fractions using the GRIM method. DT showed well-defined lamellar microdomains in bulk confirmed by SAXS. The thin film morphology measured by using AFM and GIWAXS showed parallel oriented lamellar microdomains, while P3DDT fibrils were observed on the top of the film surface. Thus, the films showed end-on orientation throughout the film, although edge-on orientation existed in P3DDT fibrils locating at the film surface.

DT showed much improved hole mobility along the film thickness direction compared with neat P3DDT film in spite of presence of P3TEGT block with low hole mobility. This indicates that end-on orientation is very effective in improving the hole mobility along the vertical direction of the films. Once one can design lamellar forming block copolymers having higher mobility than P3DDT and P3TEGT, much higher hole mobility could be expected, which is very useful for designing high performance vertically operating devices.

ASSOCIATED CONTENT

Supporting Information

The Supporting Information is available free of charge on the ACS Publications website at DOI: 10.1021/acs.macromol.9b01266.

^{1}H NMR spectrum of TEGT monomer and DT-48, SEC traces, SAXS, WAXS, GIWAXS, XRR, and DSC thermograms for homopolymers and P3DDT-*b*-P3TEGT, AFM images and GISAXS of DT-65 (PDF)

AUTHOR INFORMATION

Corresponding Author

*E-mail jkkim@postech.ac.kr.

ORCID

Kilwon Cho: 0000-0003-0321-3629

Hong Chul Moon: 0000-0003-2598-0925

Jin Kon Kim: 0000-0002-3872-2004

Author Contributions

K.S.L. and P.K. contributed equally to this work.

Notes

The authors declare no competing financial interest.

ACKNOWLEDGMENTS

This work was supported by the National Creative Research Initiative Program supported by the National Research Foundation of Korea (2013R1A3A2042196). SAXS (WAXS), GISAXS (GIWAXS), and XRR experiments were done at the 4C, 3C, and 5A beamlines of PAL (Korea), respectively.

REFERENCES

(1) Sirringhaus, H.; Tessler, N.; Friend, R. H. Integrated optoelectronic devices based on conjugated polymers. *Science* **1998**, *280*, 1741−1744.

(2) Sauve, G.; McCullough, R. D. High field-effect mobilities for diblock copolymers of poly(3-hexylthiophene) and poly(methyl acrylate). *Adv. Mater.* **2007**, *19*, 1822−1825.

(3) Zhu, M.; Pan, S.; Wang, Y.; Tang, P.; Qiu, F.; Lin, Z.; Peng, J. Unravelling the Correlation between Charge Mobility and Cocrystallization in Rod-Rod Block Copolymers for High-Performance Field-Effect Transistors. *Angew. Chem.* **2018**, *130*, 8780−8784.

(4) Woo, C. H.; Thompson, B. C.; Kim, B. J.; Toney, M. F.; Frechet, J. M. J. The Influence of Poly(3-hexylthiophene) Regioregularity on Fullerene-Composite Solar Cell Performance. *J. Am. Chem. Soc.* **2008**, *130*, 16324−16329.

(5) Zhu, M.; Kim, H.; Jang, Y. J.; Park, S.; Ryu, D. Y.; Kim, K.; Tang, P.; Qiu, F.; Kim, D. H.; Peng, J. Toward high efficiency organic photovoltaic devices with enhanced thermal stability utilizing P3HT-*b*-P3PHT block copolymer additives. *J. Mater. Chem. A* **2016**, *4*, 18432−18443.

(6) McQuade, D. T.; Pullen, A. E.; Swager, T. M. Conjugated polymer-based chemical sensors. *Chem. Rev.* **2000**, *100*, 2537−2574.

(7) Wang, Y.; Cui, H.; Zhu, M.; Qiu, F.; Peng, J.; Lin, Z. Tailoring Phase Transition in Poly(3-hexylselenophene) Thin Films and Correlating Their Crystalline Polymorphs with Charge Transport properties for Organic Field-Effect Transistors. *Macromolecules* **2017**, *50*, 9674−9682.

(8) He, Y.; Pang, X.; Jiang, B.; Feng, C.; Harn, Y. W.; Chen, Y.; Yoon, Y. J.; Pan, S.; Lu, C. H.; Chang, Y.; Zebarjadi, M.; Kang, Z.; Thadhani, N.; Peng, J.; Lin, Z. Unconventional Route to Uniform Hollow Semiconducting Nanoparticles with Tailorable Dimensions, Compositions, Surface Chemistry, and Near-Infrared Absorption. *Angew. Chem.* **2017**, *129*, 13126−13131.

(9) Topham, P. D.; Parnell, A. J.; Hiorns, R. C. Block Copolymer Strategies for Solar Cell Technology. *J. Polym. Sci., Part B: Polym. Phys.* **2011**, *49*, 1131−1156.

(10) Segalman, R. A.; McCulloch, B.; Kirmayer, S.; Urban, J. J. Block Copolymers for Organic Optoelectronics. *Macromolecules* **2009**, *42*, 9205−9216.

(11) Yu, J. S.; Zheng, Y. F.; Huang, J. Towards High Performance Organic Photovoltaic Cells: A Review of Recent Development in Organic Photovoltaics. *Polymers* **2014**, *6*, 2473−2509.

(12) Ma, J. S.; Hashimoto, K.; Koganezawa, T.; Tajima, K. End-On Orientation of Semiconducting Polymers in Thin Films Induced by Surface Segregation of Fluoroalkyl Chains. *J. Am. Chem. Soc.* **2013**, *135*, 9644−9647.

(13) Lim, J. A.; Liu, F.; Ferdous, S.; Muthukumar, M.; Briseno, A. L. Polymer semiconductor crystals. *Mater. Today* **2010**, *13*, 14−24.

(14) Aryal, M.; Trivedi, K.; Hu, W. C. Nano-Confinement Induced Chain Alignment in Ordered P3HT Nanostructures Defined by Nanoimprint Lithography. *ACS Nano* **2009**, *3*, 3085−3090.

(15) Agostinelli, T.; Lilliu, S.; Labram, J. G.; Campoy-Quiles, M.; Hampton, M.; Pires, E.; Rawle, J.; Bikondoa, O.; Bradley, D. D. C.; Anthopoulos, T. D.; Nelson, J.; Macdonald, J. E. Real-Time Investigation of Crystallization and Phase-Segregation Dynamics in P3HT:PCBM Solar Cells During Thermal Annealing. *Adv. Funct. Mater.* **2011**, *21*, 1701−1708.

(16) Li, G.; Yao, Y.; Yang, H.; Shrotriya, V.; Yang, G.; Yang, Y. Solvent annealing" effect in polymer solar cells based on poly(3-hexylthiophene) and methanofullerenes. *Adv. Funct. Mater.* **2007**, *17*, 1636−1644.

(17) Liao, H. C.; Ho, C. C.; Chang, C. Y.; Jao, M. H.; Darling, S. B.; Su, W. F. Additives for morphology control in high-efficiency organic solar cells. *Mater. Today* **2013**, *16*, 326−336.

(18) Kim, J. S.; Park, Y.; Lee, D. Y.; Lee, J. H.; Park, J. H.; Kim, J. K.; Cho, K. W. Poly(3-hexylthiophene) Nanorods with Aligned Chain Orientation for Organic Photovoltaics. *Adv. Funct. Mater.* **2010**, *20*, 540−545.

(19) Skrypnychuk, V.; Boulanger, N.; Yu, V.; Hilke, M.; Mannsfeld, S. C. B.; Toney, M. F.; Barbero, D. R. Enhanced Vertical Charge Transport in a Semiconducting P3HT Thin Film on Single Layer Graphene. *Adv. Funct. Mater.* **2015**, *25*, 664−670.

(20) Jimison, L. H.; Toney, M. F.; McCulloch, I.; Heeney, M.; Salleo, A. Charge-Transport Anisotropy Due to Grain Boundaries in Directionally Crystallized Thin Films of Regioregular Poly(3-hexylthiophene). *Adv. Mater.* **2009**, *21*, 1568−1572.

(21) Higashihara, T.; Ohshimizu, K.; Ryo, Y.; Sakurai, T.; Takahashi, A.; Nojima, S.; Ree, M.; Ueda, M. Synthesis and characterization of block copolythiophene with hexyl and triethylene glycol side chains. *Polymer* **2011**, *52*, 3687−3695.

(22) Higashihara, T.; Ohshimizu, K.; Hirao, A.; Ueda, M. Facile Synthesis of ABA Triblock Copolymer Containing Regioregular

DOI: 10.1021/acs.macromol.9b01266
Macromolecules 2019, 52, 6734−6740

Poly(3-hexylthiophene) and Polystyrene Segments via Linking Reaction of Poly(styryl)lithium. *Macromolecules* **2008**, *41*, 9505−9507.
(23) Moon, H. C.; Anthonysamy, A.; Lee, Y.; Kim, J. K. Facile Synthesis of Well-Defined Coil-Rod-Coil Block Copolymer Composed of Regioregular Poly(3-hexylthiophene) via Anionic Coupling Reaction. *Macromolecules* **2010**, *43*, 1747−1752.
(24) Moon, H. C.; Anthonysamy, A.; Kim, J. K.; Hirao, A. Facile Synthetic Route for Well-Defined Poly(3-hexylthiophene)-*block*-poly(methyl methacrylate) Copolymer by Anionic Coupling Reaction. *Macromolecules* **2011**, *44*, 1894−1899.
(25) Choi, S. Y.; Lee, J. U.; Lee, J. W.; Lee, S.; Song, Y. J.; Jo, W. H.; Kim, S. H. Highly Ordered Poly(3-hexylthiophene) Rod Polymers via Block Copolymer Self-Assembly. *Macromolecules* **2011**, *44*, 1771−1774.
(26) Lee, K. S.; Lee, J. Y.; Choi, C. R.; Seo, Y. S.; Moon, H. C.; Kim, J. K. Vertically Oriented Nanostructures of Poly(3-dodecylthiophene)-Containing Rod-Coil Block Copolymers. *Macromolecules* **2018**, *51*, 4956−4965.
(27) Shao, M.; He, Y. J.; Hong, K. L.; Rouleau, C. M.; Geohegan, D. B.; Xiao, K. A water-soluble polythiophene for organic field-effect transistors. *Polym. Chem.* **2013**, *4*, 5270−5274.
(28) Lee, Y. H.; Yang, Y. L.; Yen, W. C.; Su, W. F.; Dai, C. A. Solution self-assembly and phase transformations of form II crystals in nanoconfined poly (3-hexyl thiophene) based rod-coil block copolymers. *Nanoscale* **2014**, *6*, 2194−2200.
(29) Maher, M. J.; Self, J. L.; Stasiak, P.; Blachut, G.; Ellison, C. J.; Matsen, M. W.; Bates, C. M.; Willson, C. G. Structure, Stability, and Reorganization of 0.5 L-0 Topography in Block Copolymer Thin Films. *ACS Nano* **2016**, *10*, 10152−10160.
(30) Hu, H. Q.; Gopinadhan, M.; Osuji, C. O. Directed SelfAssembly of Block Copolymers: A Tutorial Review of Strategies for Enabling Nanotechnology with Soft Matter. *Soft Matter* **2014**, *10*, 3867−3889.
(31) Park, J.; Lee, K. S.; Choi, C.; Kwak, J.; Moon, H. C.; Kim, J. K. Effect of Molecular Weight on Competitive Self-Assembly of Poly(3-Dodecylthiophene)-Block-Poly(Methyl Methacrylate) Copolymers. *Macromolecules* **2016**, *49*, 3647−3653.
(32) Ihn, K. J.; Moulton, J.; Smith, P. Whiskers of Poly(3-alkylthiophene)s. *J. Polym. Sci., Part B: Polym. Phys.* **1993**, *31*, 735−742.
(33) Kaus, N. H. M.; Collins, A. M.; Bikondoa, O.; Cresswell, P. T.; Bulpett, J. M.; Briscoe, W. H.; Mann, S. In situ X-ray reflectivity studies of molecular and molecular-cluster intercalation within purple membrane films. *J. Mater. Chem. C* **2014**, *2*, 5447−5452.
(34) Lorenzo, A.; Marmisolle, W. A.; Maza, E. M.; Ceolin, M.; Azzaroni, O. Electrochmical nanoarchitectonics through polyaminobenzylamine-dodecyl phosphate complexes: redox activity and mesoscopic organization in self-assembled nanofilms. *Phys. Chem. Chem. Phys.* **2018**, *20*, 7570−7578.
(35) Zhang, J.; Posselt, D.; Smilgies, D.; Perlich, J.; Kyriakos, K.; Jaksch, S.; Papadakis, C. M. Lamellar Diblock Copolymer Thin Films during Solvent Vapor Annealing Studied by GISAXS: Different Behavior of Parallel and Perpendicular Lamellae. *Macromolecules* **2014**, *47*, 5711−5718.
(36) Su, Y. W.; Lin, Y. C.; Wei, K. H. Evolving molecular architectures of donor-acceptor conjugated polymers for photovoltaic applications: From one-dimensional to branched to two-dimensional structures. *J. Mater. Chem. A* **2017**, *5*, 24051−24075.
(37) Matsen, M. W. The standard Gaussian model for block copolymer melts. *J. Phys.: Condens. Matter* **2002**, *14*, R21−R47.
(38) Cheng, L.; Cao, D. Understanding self-assembly of rod-coil copolymer in nanoslits. *J. Chem. Phys.* **2008**, *128*, 074902.
(39) Bass, J. Deviations from Matthiessen's Rule. *Adv. Phys.* **1972**, *21*, 431−604.

DOI: 10.1021/acs.macromol.9b01266
Macromolecules 2019, 52, 6734−6740